*Progress In Electromagnetics Research C, Vol. 120, 61–75, 2022*

# Efficient Indoor Wireless Monitoring of Long-Term Ill/Post Operative Patients with Implants

**Samuelraj Chrysolite*** **and Anita Jones Mary Pushpa**

**Abstract**—In the medical world, the continuous monitoring of patients having a long-term illness is mandatory. The usual monitoring systems placed around the patients are bulkier and costly. Moreover, the movement of those patients is limited as they are connected to the monitoring devices with probes. To enable the locomotion of the patients a miniaturized implantable antenna sensor with the dimension $2.5 \times 7 \times 0.25\,\text{mm}^3$ is proposed to monitor arterial pressure. The proposed antenna sensor is fabricated and verified for its performance metrics. Radiation analysis for the implants is carried out through a metric called Specific Absorption Rate (SAR). Deviation of pressure in the patient is measured through the rate of change of resonant frequency through an external reader coil. Communication established between the Transmitter (patient with implant) and the Receiver for better monitoring is verified through field strength calculated at various locations inside the hospital rooms in order to allocate rooms for the post-operative/long term ill patients efficiently.

## 1. INTRODUCTION

Implants are becoming an essential part of our everyday life ranging from medical applications [1] to individual tracking [2]. These implants communicate wirelessly and also enable the building of databases when continuously monitoring a particular attribute inside the body. Recently, implantable antennas have been designed with biocompatible materials like silicon wafer as a substrate and copper as a radiating patch [3] for monitoring various attributes like pressure, temperature, and heart rate. They also emphasize encapsulation with materials like Silicone/Polyurethane composites [4] or even coat the bio-polymers to reduce the amount of infection which happens after implantation (fibrosis) [5]. Many researchers reported designs of implantable antennas tested in-vivo and in-vitro [6]. As implants are ingestible/injectible, radiation exposure is measured by a metric called Specific Absorption Rate (SAR) [7]. Various ingestible antennas were reviewed upon, and the state of art was expressed in terms of flexibility analysis [8]. Many biodegradable implants for pressure monitoring have been proposed by many researchers. Copper and Poly-Lactic Acid (PLA) were used to design an RFID tag to detect early stages of infection [9]. Magnesium along with biodegradable polymers like Poly-Glycerol Sebacate (PGS) and Poly-L-Lactic Acid (PLLA) are used for fabricating pressure and strain monitoring sensors used in monitoring tendon healing [10]. Magnesium and biodegradable polymers like PLLA are used for fabricating pressure monitoring sensors in monitoring pressure in the arteries [11].

Long-term ill patients need more care and also some space for their own to recover from it. The basic monitoring systems which are very bulky [12], and also the inter-connection probes enforce restrictions on the movement of those patients [13]. To enable the patient's movement, a mobile monitoring system was developed [14]. Various mobile patient monitoring systems are compared to overcome the challenges like place and interference constraints [15]. But still all probes were needed to be connected with the

*Received 29 January 2022, Accepted 18 April 2022, Scheduled 6 May 2022*
* Corresponding author: Samuelraj Chrysolite (g.samuelraj@gmail.com).
The authors are with the Electronics and Communication Engineering, Karunya University, Coimbatore, India.

patient even though the monitoring system was mobile. Hence, a wireless pressure monitoring implant is proposed for a postoperative patient where the efficiency of the monitoring is of utmost importance.

Section 2.1 emphasizes the methodology behind the antenna design and its geometry parameters. Section 2.2 discusses the indoor monitoring scenario based on the hospital site (IP block) considered. Section 3.1 tabulates the results based on the optimization path of the initial design. Section 3.2 briefs upon the various performance analysis of the proposed design (simulated & fabricated) followed by the field strength based analysis inside the hospital at various positions of the patients in Section 3.3. Conclusion and future works are discussed in Section 4.

## 2. METHODOLOGY

### 2.1. Antenna Geometry

A novel implantable spiral antenna is designed with dimension $2.5 \times 7 \times 0.25$ cubic mm as per the design parameters tabulated in Table 1 according to the transmission line model [19]. The geometry of the miniaturized antenna is depicted in Figures 1(a), 1(b), and the antenna is designed and simulated using ALTAIR FEKO with finite difference time domain (FDTD) solver activated. The FDTD solver defines the boundary condition and is set as open on all sides of the designed antenna. A free space buffer is automatically added on all sides based on the proposed antenna design. The designed antenna has an

**Table 1.** Design parameters.

| Parameters | Variables | Value (mm) |
|---|---|---|
| Substrate Width | $sw$ | 2.25 |
| Substrate Depth | $sd$ | 7 |
| Substrate Depth (Left Side) | $sd\_ls$ | 7 |
| Patch Width | $pw$ | 0.29 |
| Substrate Width (Port Side) | $sw\_ps$ | 0.7 |
| Substrate Height | $sh$ | 0.25 |
| Superstrate Height | $ss\_h$ | 0.25 |

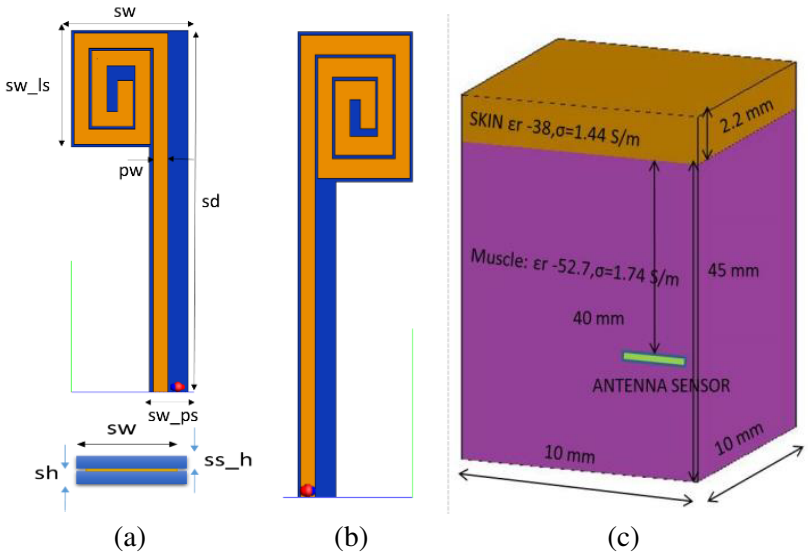


**Figure 1.** Geometry of the proposed antenna sensor. (a) Ventral view. (b) Dorsal view. (c) Implant surrounding.

RT DUROID 6010 substrate and a copper radiating patch. The implant surrounding is simulated as shown in Figure 1(c) with the necessary dielectric properties [18]. The muscle and skin are taken into account with epsilon ($r$) of 52.7 and 38, respectively, for simulation purpose. The length and width of the radiating patch are calculated based on Eqs. (1) and (2) [19].

$$W = \frac{v_0}{2f_r}\sqrt{\frac{2}{\varepsilon_r + 1}} \tag{1}$$

$f_r$ — Resonant Frequency, $v_0$ — Velocity of light, $\varepsilon_r$ — Relative permittivity of substrate

$$L = \frac{1}{2f_r\sqrt{\varepsilon_{reff}}\sqrt{\mu_0\varepsilon_0}} - 2\Delta L \tag{2}$$

$L$ — Length of the patch, $f_r$ — Resonant Frequency, $\varepsilon_0$ — Relative permittivity of air, $\mu_0$ — Relative permeability of air, $\varepsilon_{reff}$ — Effective value of the dielectric substrate. The fringing fields present around the microstrip patch antenna alter the dielectric constant, thereby altering the length of the patch ($\Delta L$) (3) [19]. The effective length of the dielectric substrate is calculated by adding twice of the change in length with the original length $L$ (4) [19]. The effective dielectric constant is given by Eq. (5) [19].

$$\Delta L = 0.412h\frac{(\varepsilon_{reff} + 0.3)\left(\frac{W}{h} + 0.264\right)}{(\varepsilon_{reff} - 0.258)\left(\frac{W}{h} + 0.8\right)} \tag{3}$$

$$L_{eff} = L + 2\Delta L \tag{4}$$

$$\varepsilon_{reff} = \frac{\varepsilon_r + 1}{2} + \frac{\varepsilon_r - 1}{2}\left[1 + 12\frac{h}{W}\right]^{-\frac{1}{2}} \tag{5}$$

As the length of the patch has been extended by $\Delta L$ on each side, the effective length of the patch is $\lambda/2$ for dominant TM010 mode. The physical length and width of the patch are calculated as 6.97 and 0.29 mm. The input is given through a wire feed, and the feed location $(X, Y)$ is calculated by Eqs. (6) and (7) for good impedance matching [20]. The position is calculated based on the effective dielectric constant which alters the impedance at various positions of the proposed antenna design.

$$X = \frac{L}{\sqrt[2]{\varepsilon_{reff}}} \tag{6}$$

$$Y = \frac{W}{2} \tag{7}$$

The proposed antenna is small enough to fit in the wrist of the patient and operates at a frequency of 2.45 GHz. The ground and radiating patch share a common geometry. The thickness of the substrate/superstrate (RT Duroid 6010) is 0.25 mm. The width of the patch is varied to improve the current flow from the wire port towards the terminated end of the radiating patch. The ground is designed similar to the radiating patch to tune the antenna towards the 2.45 GHz band. To get better radiation characteristics, the length and width of the rectangular radiating loop are varied which enables better flow of current from the source through the radiating patch. Shorting pins are also used to increase the distance of current flow thereby achieving good radiation even in a very small area of design. The capacitive difference between the patch and ground causes a shift in the resonance frequency. The change in the resonance frequency $\Delta f_r$ is substantiated by Eq. (8) [11].

$$\Delta f_r = -\frac{\Delta C}{4\pi\sqrt{LC^3}} \tag{8}$$

$\Delta f_r$ — Rate of change of resonant frequency, $\Delta C$ — Rate of change of capacitance, $C$ — Capacitive Load, $L$ — Inductive Load. The change in resonance depends upon the capacitance and the inductance values between the radiating patch and the ground. The change in capacitance can be controlled by increasing/decreasing the area of the radiating patch in contact with the ground plane (9) [19].

$$C = \frac{A\varepsilon_0}{d} \tag{9}$$

$C$ — Capacitive Load, $A$ — Area of radiating patch, $\varepsilon_0$ — Relative permittivity of air, $d$ — Distance between the radiating patch and the ground. Sensitivity of the device is increased by increasing the area of the patch in contact with the ground. The capacitive load determines the rate of change in resonant frequency. If the pressure is high, the the range of frequency shift is minimum and vice-versa when the pressure is low. The change in the rate of frequency shift and the range of the resonant frequency fluctuations at the reader coil are used to calculate the pressure values [16]. The capacitive load does not affect the response time of the pressure monitoring implant [11].

SAR values are calculated by Eq. (10), according to the ICNIRP standard for 10 g SAR which should be less than 2 W/kg [17].

$$\mathrm{SAR} = \frac{\sigma\,|E|^2}{\rho} \tag{10}$$

where SAR — Specific Absorption Rate, $\sigma$ — Conductivity, $E$ — Internal Electric Field (Root Mean Square Value), $\rho$ = Mass Density. $\mathrm{SAR}_{10\,\mathrm{g}}$ is defined as the total power absorbed in a 10-g cubic volume divided by 10 g (11). A 10-g volume ($V_{10\,\mathrm{g}}$) is approximately computed as a 2.15 cm × 2.15 cm × 2.15 cm cube, based on the assumption that the tissue has the same mass density as water, or 1,000 kg m$^{-3}$.

$$\mathrm{SAR}_{10\,\mathrm{g}} = \frac{(\mathrm{Total\,Power})_{10\,\mathrm{g}}}{(\mathrm{Total\,Mass})_{10\,\mathrm{g}}} = \frac{\left[\int \sigma\,|E|^2\,dv\right]_{V_{10\,\mathrm{g}}}}{\int \rho dv} \tag{11}$$

## 2.2. Indoor Scenario

The proposed antenna for long term ill patients as an implant for pressure monitoring is verified by creating an indoor scenario of a hospital inpatient ward with two floors designed using FEKO Wall man (ALTAIR). Each floor is designed with 10 rooms for the ease of simulation. The width and length of each room considered for the aforementioned scenario are approximately 9 m × 6 m. The material characteristics are kept to default (concrete). The schematic layouts of the Ground floor, First floor and Second floor of the inpatient ward are shown as Figures 2(a), (b), & (c). The dimensions of a single

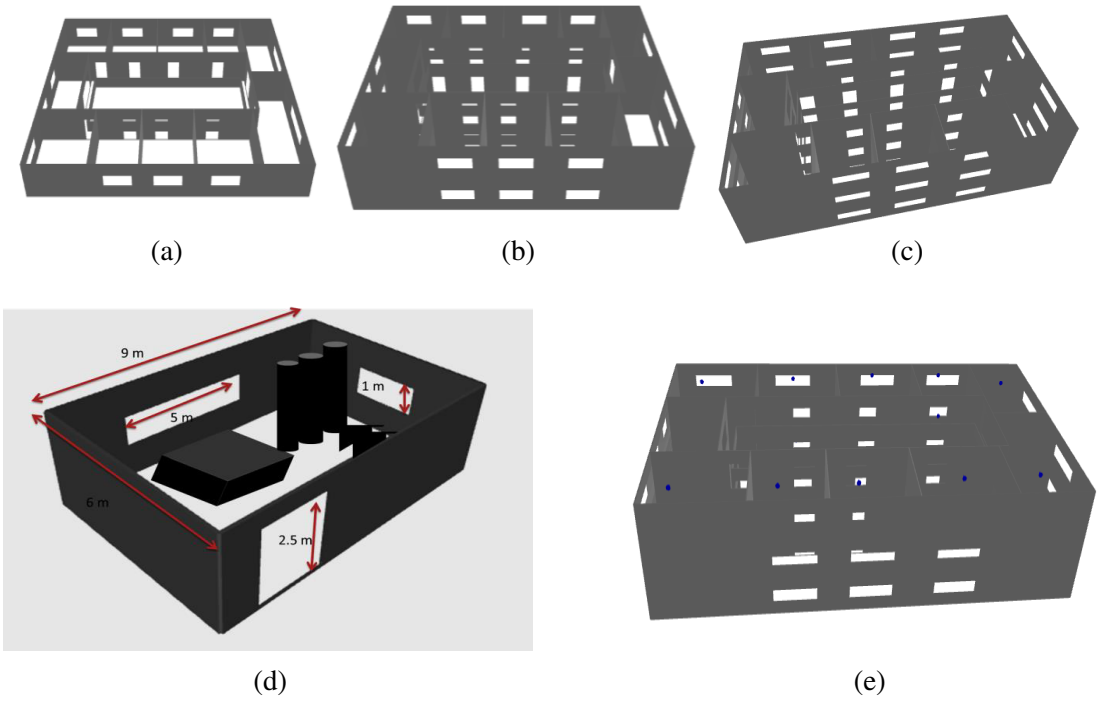


**Figure 2.** Design of various floors of the inpatient ward. (a) Ground floor. (b) First floor. (c) Second floor. (d) Scenario of a single room. (e) Hospital in-patient ward with transmitter.

room are shown in Figure 2(d). The inpatient ward with the implantable antennas placed in each room of the second floor for analyzing the field strength is shown in Figure 2(e).

The walls are designed with a thickness of 15 cm. The windows and doors of each room are placed in a random manner. The windows are of 5 m × 1 m in dimension. Regular doors are designed with a thickness of 2 inches. Furniture present in each room is also designed. A staircase is designed connecting all the floors on the left hand side of the building. A common balcony is designed in the center enabling easy access for the wheelchairs and rolling beds. Each floor has a height of 3 m.

The implantable antenna's viability is analyzed in each room taking into account the presence of the patient and all other materials (metals) present in the room. The implantable antenna is placed at a height of 1.5 m from the floor (prediction plane). The static receiver is set at the center of the building.

## 3. RESULTS & DISCUSSION

### 3.1. Optimized Design

#### *3.1.1. Varying the Patch Length*

When the length of the radiating loop is increased, an increase in the distance of flow of current is observed, resulting in a better reflection coefficient at the resonant frequency as shown in Figures 3(a), 3(b), 3(c), & 3(d). When the rectangular loop's length is increased, the number of loops in the rectangular spiral also increases.

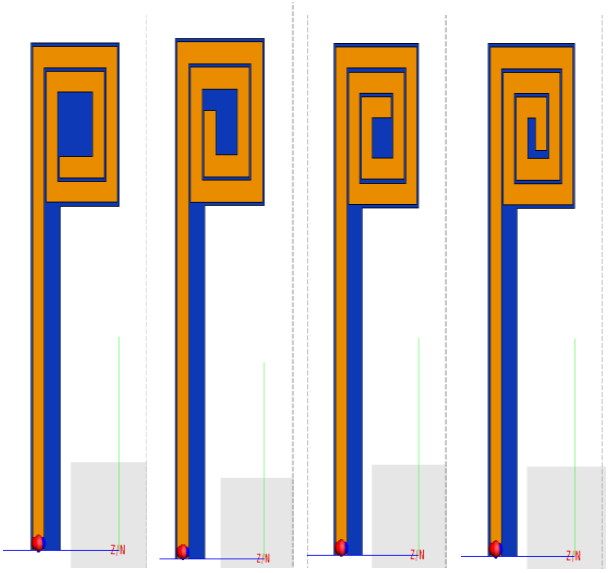


**Figure 3.** Varying the length of the radiating patch. (a) Design 1. (b) Design 2. (c) Design 3. (d) Design 4.

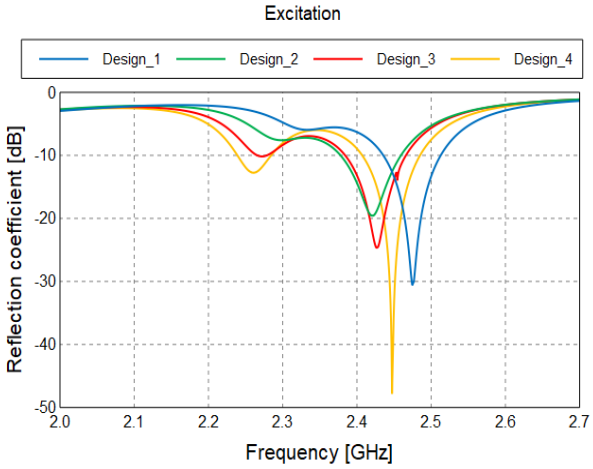


**Figure 4.** Comparison by varying the length of the radiating patch.

A comparison graph is plotted for various lengths of the radiating loop as shown in Figure 4. When the patch length is increased, an initial increase in the reflection coefficient is observed which then drops significantly. A resonant frequency shift is observed when the length of the radiating patch at the ground is varied. It is due to the variation of the distance that the electromagnetic waves have traveled before radiation. Parameters like reflection coefficient, VSWR, realized gain, and impedance for various lengths of the radiating loop are tabulated in Table 2. According to the analysis, Design 4 with four loops performs better than the other designs considered.

**Table 2.** Antenna parameters while varying the length of the radiating patch.

| Antenna parameters | Design 1 | Design 2 | Design 3 | Design 4 |
|---|---|---|---|---|
| Reflection Coefficient (dB) | −30.75 | −19.60 | −24.71 | −60.57 |
| VSWR (dB) | 1.57 | 1.66 | 3.46 | 1.07 |
| Realized Gain (dBi) | −47.36 | −59.49 | −42.34 | −39.39 |
| Impedance (Ω) | 69.6 | 34.1 | 36.7 | 49 |

### *3.1.2. Varying the Patch Width*

When the width of the patch is increased/decreased, an accumulation of electric charges at the terminated end is observed, which thereby increases/decreases the output gain of the antenna as shown in Figures 5(a), (b), (c), (d). A comparison graph is plotted for various widths of the radiating loop as shown in Figure 6. When the patch width is increased, a decrease in the reflection coefficient is observed.

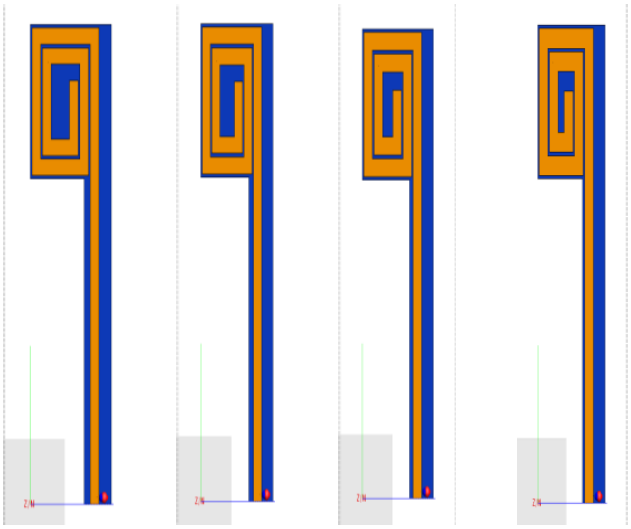


**Figure 5.** Varying the width of the radiating patch. (a) Design 1. (b) Design 2. (c) Design 3. (d) Design 4.

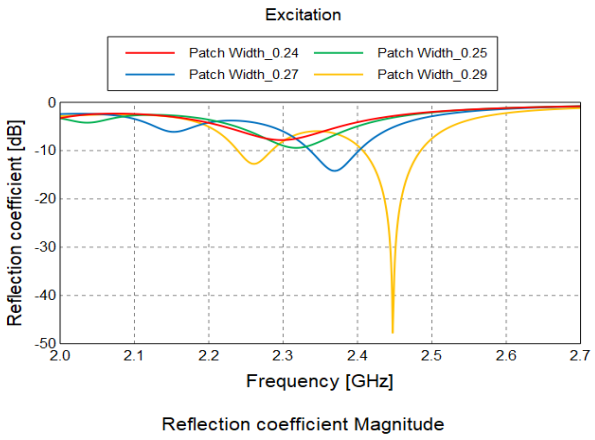


**Figure 6.** Comparison by varying the width of the radiating patch.

**Table 3.** Antenna parameters while varying the width of the radiating patch.

| Antenna parameters | Design 1 $p\_d = 0.24$ mm | Design 2 $p\_d = 0.25$ mm | Design 3 $p\_d = 0.27$ mm | Proposed Design $p\_d = 0.29$ mm |
|---|---|---|---|---|
| Reflection Coefficient (dB) | −7.81 | −9.42 | −14.2 | −60.57 |
| VSWR (dB) | 15.91 | 15 | 10.9 | 1.07 |
| Realized Gain (dBi) | −66.36 | −58.49 | −50.34 | −39.39 |
| Impedance (Ω) | 13.6 | 13.6 | 14.8 | 49 |

It is because there must be a certain amount of traffic of the charges flowing in the radiating patch. The charges flowing through should not be scarce, or should not get accumulated due to heavy traffic. So when the width is increased beyond the threshold, an increase in the reflection coefficient is observed, which leads to poor radiation characteristics. Parameters like reflection coefficient, VSWR, realized gain, and impedance for various widths of the radiating loop are tabulated in Table 3. According to the analysis, Design 4 with patch width of 0.29 mm performs better than the other designs considered.

## 3.2. Analysis of Proposed Design

As per the aforementioned results, Design 4 performs well in all the characteristics analysis. Therefore, the results are discussed below with patch width — 0.29 mm and number of loops as four. Various parameters like reflection coefficient, realized gain, VSWR, impedance matching, and current distribution are analyzed.

### *3.2.1. Reflection Coefficient*

In Figure 7, a reflection coefficient of −60.57 dB is achieved which is sufficient enough for the antenna to be implanted. A narrow bandwidth of 40.89 MHz at −15 dB is achieved enabling an efficient data transmission to the output reader.

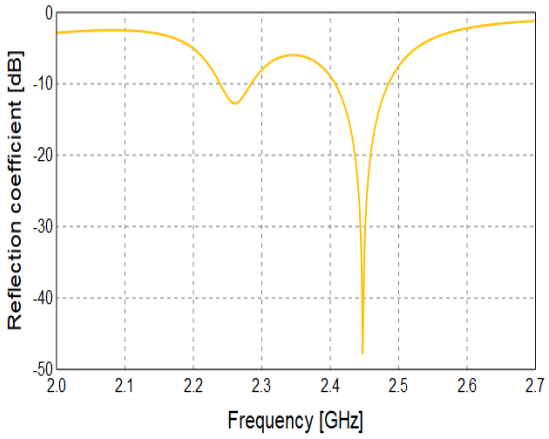


**Figure 7.** Reflection coefficient of the proposed design.

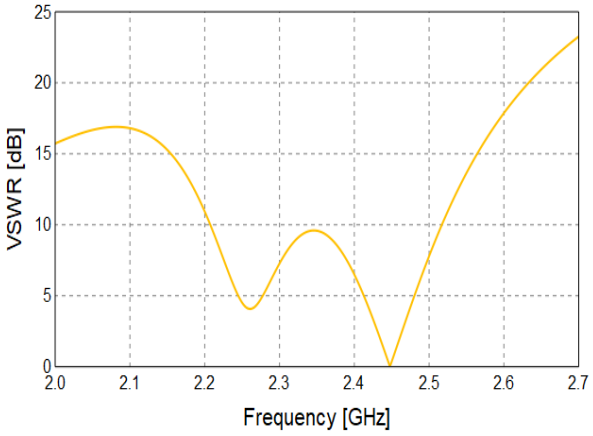


**Figure 8.** VSWR of the proposed design.

### *3.2.2. Voltage Standing Wave Ratio*

The voltage standing wave ratio at 2.45 GHz is 0.188 dB which suggests that the standing waves are very low enabling maximum radiation as shown in Figure 8. It prevents the cancellation of the electromagnetic waves traveling through the antenna medium thereby resulting in efficient radiation.

### *3.2.3. Realized Gain*

Gain plays a major role in providing efficient data to a sufficient distance for easier reception by the receiver antenna. In Figure 9, at 2.45 GHz a realized gain −36.39 dBi is achieved which has an efficient transmission range of 20 m. The range is good enough for continuous monitoring of the patient.

### *3.2.4. Impedance*

The impedance matching depicts the free flow of current in the radiating patch. At a reference impedance of 50 Ohm, the mismatch is very low, and an impedance (49 Ohm) equivalent to the reference is achieved as in Figure 10, which shows that the current flow is good.

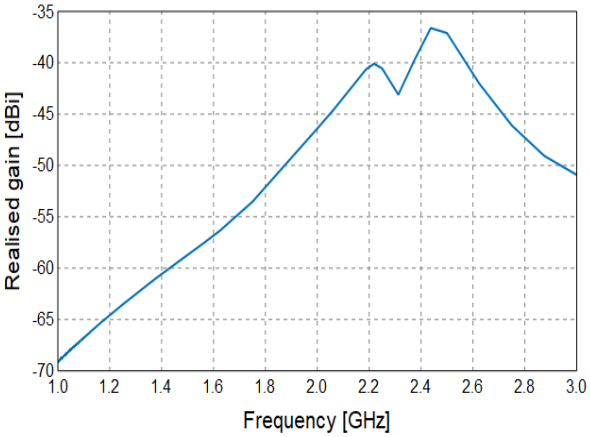


**Figure 9.** Realized gain of the proposed design.

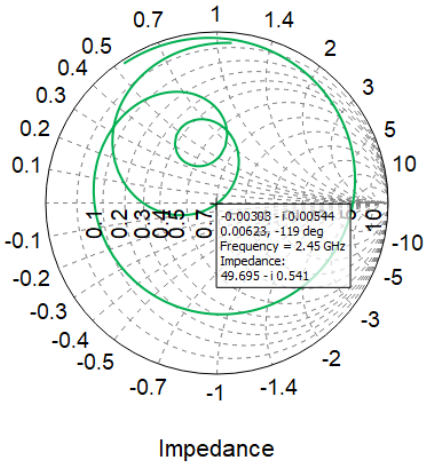


**Figure 10.** Impedance of the proposed design.

### *3.2.5. Current Distribution*

The current distribution is also a major factor in determining the resonant frequency and reflection coefficient of the implantable antenna. Hence even distribution of the same is focused upon. To ease the accumulation of current in a particular place on the radiating patch, shorting pins are used. The current distribution at 2.45 GHz is shown in Figure 11(a).

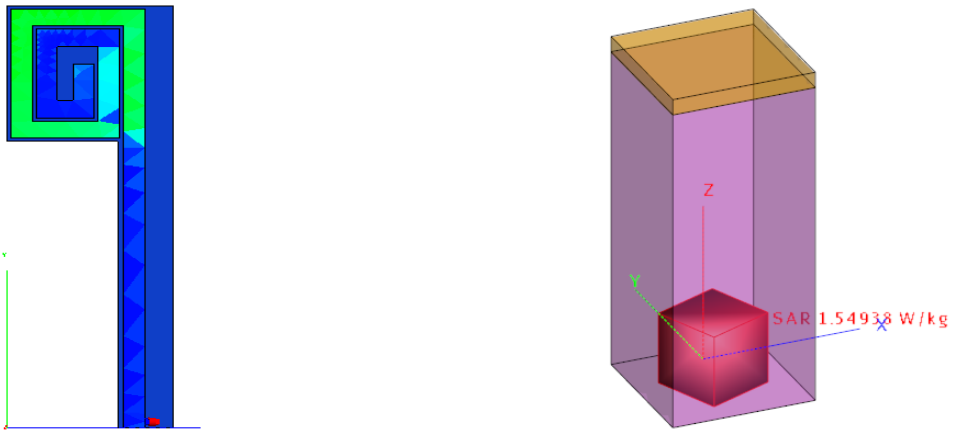


(a) (b)

**Figure 11.** (a) Current distribution of the proposed design. (b) 10 g specific absorption rate ($SAR_{10\,g}$).

### *3.2.6. Specific Absorption Rate ($SAR_{10\,g}$)*

The specific absorption rate (10 g) of an implantable antenna should be less than 2 W/kg without uncertainties according to the ICNIRP standards [17]. For the proposed design at resonant frequency of 2.45 GHz, at a depth of 40 mm from the skin, for the defined FDTD boundary conditions, a 10 g SAR of 1.549 W/kg (Input Power — 5 mW) is recorded which is well within the standard exposure limits [17] as in Figure 11(b).

### *3.2.7. 2-D & 3-D Pattern*

The 2-D pattern and 3-D pattern of the far-field distribution are also plotted as shown in Figures 12(a) and (b). The pattern shows an omnidirectional distribution and is suitable for the proposed application. At 2.45 GHz, a gain of −36.39 dBi is achieved as shown in Figure 12(a).

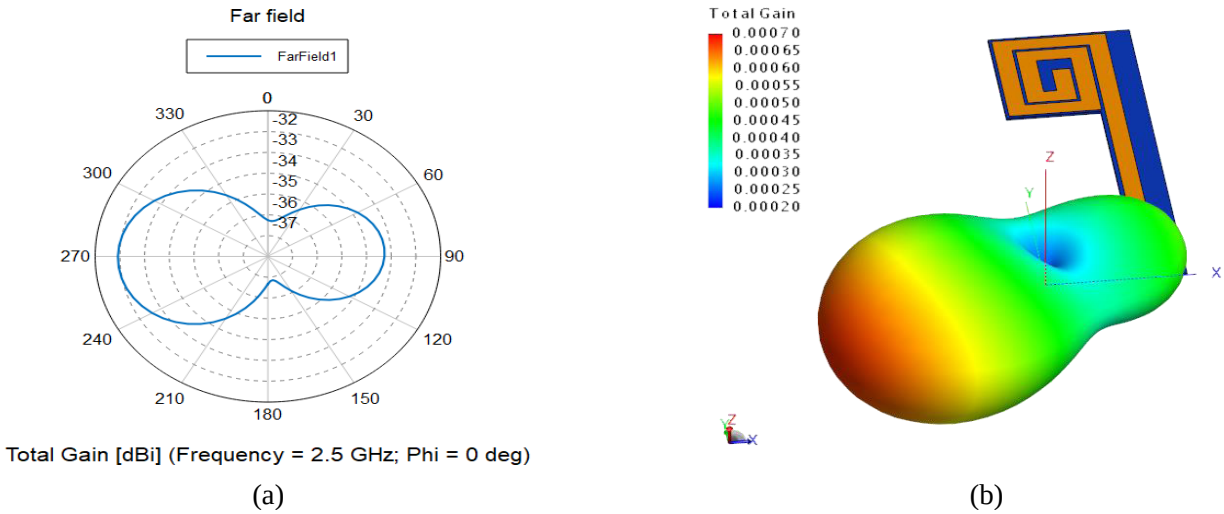


**Figure 12.** (a) 2-D pattern of the proposed design. (b) 3-D pattern of the proposed design.

### *3.2.8. Comparative Analysis with Change in Pressure*

The change in pressure changes the capacitance which in turn defines the shift in resonant frequency at the antenna reader. The shift in resonant frequency due to pressure (capacitance) change is plotted in Figure 13. A frequency shift of ∓8 MHz is seen for each capacitive change due to the pressure variation sensed by the superstrate. The area of contact between the radiating patch and substrate keeps changing for different pressure values. Therefore, the capacitance changes with respect to the input pulse given which translates into the respective resonant frequency shift at the reader. The capacitive load does not affect the response time of the pressure monitoring implant, thereby the accuracy of the biological information is also unaffected [11].

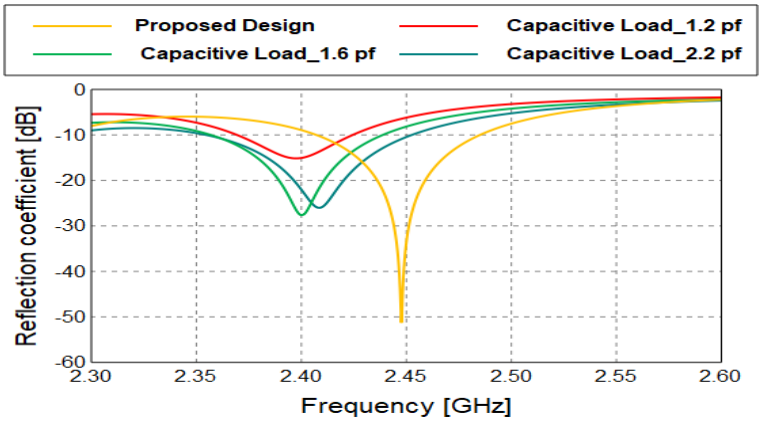


**Figure 13.** Comparison of reflection coefficient for capacitive loads.

### 3.3. Fabrication & Experimental Results

*3.3.1. Pressure Sensor*

The proposed pressure sensor was fabricated at Enthutech Solutions.pvt.Ltd with dimensions 7 mm × 2.5 mm × 0.25 mm as shown in Figures 14(a) & (b). The change in capacitive loads when the sensor is wrapped around an artery mimicking tube is realized by the change in resonant frequency at the reader coil.

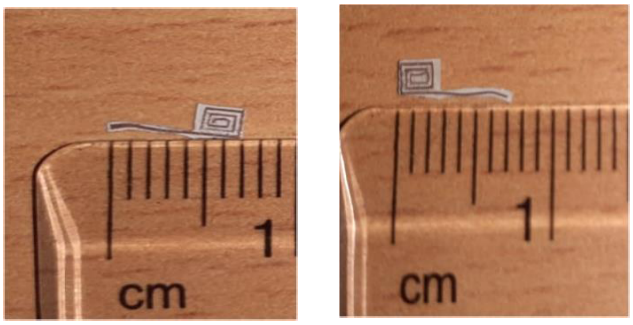


(a) (b)

**Figure 14.** Fabricated pressure sensor. (a) Front view. (b) Lateral view.

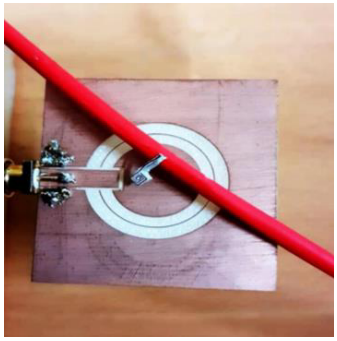

**Figure 15.** Fabricated pressure reader (front).

*3.3.2. Reader Coil*

The reader coil was fabricated at the Microwave Lab, Karunya University, designed using ALTAIR FEKO software. A coplanar concentric circular patch was considered in order to eliminate back lobes and to make the antenna an efficient one sided reader. The reader antenna is shown in Figure 15.

*3.3.3. Prototype Performance*

The sensor antenna is connected with the help of polymeric glue to a polyolefin tube of 2 mm diameter to mimic the artery. The tube with the antenna sensor is carefully placed on the flat surface. The reader connected with the Vector Network Analyzer (Microwave Labs, Karunya University) is placed near the sensor such that the capacitance change in the sensor is translated to the reader efficiently. The polyolefin tube is closed at one end, and the other end is connected to the output tube of the manual sphygmomanometer. Return loss with and without pressure inside the tube is measured. The manual sphygmomanometer is used in order to mimic the pressure inside the arteries. The prototype setup arranged with the sphygmomanometer connected to the polyolefin tube which in turn is in contact with fabricated pressure sensor is shown in Figures 16(a), (b), & (c). A comparative graph is plotted for return loss featuring the simulated and measured results. The shift in resonant frequency of the reader coil is clearly illustrated in Figure 17. Due to complexity of the in-vivo validation, the experiments were carried out in restricted environments only with the prototype setup (in air). The prototype setup, which only mimics the real environment, induces some uncertainties which is the reason behind the deviation between the measured and calculated data as seen in Figure 16.

### 3.4. Indoor Analysis

The indoor scenario as shown in Figure 2(e) is loaded as the indoor database in the Proman (FEKO) software. The third floor is taken as the reference, and transmitters depicting the proposed antenna are placed in each of the ten rooms available. The field strength for each transmitter is analyzed, and results are plotted.

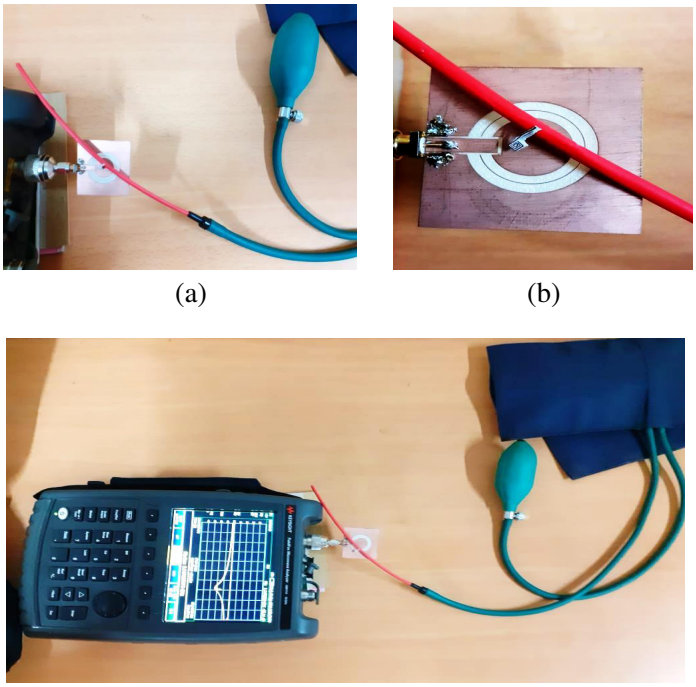


**Figure 16.** Prototype of the setup with antenna sensor and reader. (a) The antenna reader with pressure sensor. (b) The antenna sensor connected to polyolefin tube. (c) The prototype setup $n$ with VNA and sphygmomanometer.

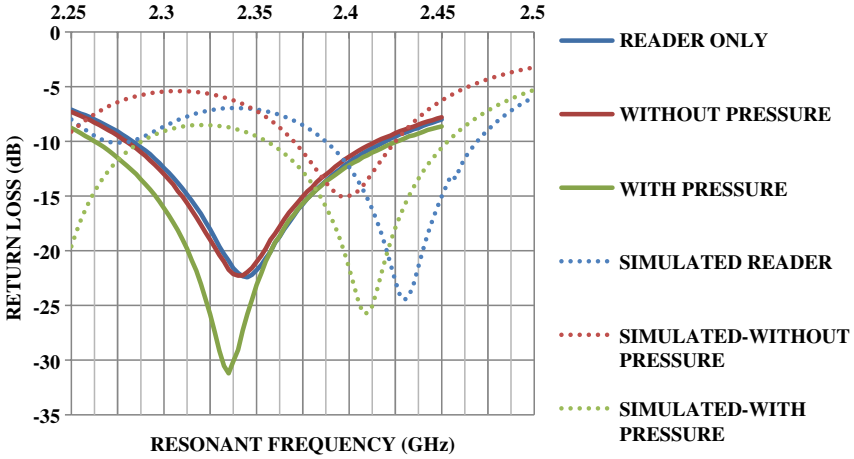


**Figure 17.** Comparison of measured and simulated results.

### *3.4.1. Analysis of Field Strength for Static Receiver*

The field strength analysis is carried out for better reception at the static receiver (nursing station for the floor). The nursing station is placed at the center, 9 m from either side of the building as shown in Figure 18. Comparative field strength from the transmitters (Input Power — 1 W) at various rooms (Room 1 to Room 10) to the nursing station placed in the center of the building on each floor is plotted as shown in Figure 19. From the graph, it is inferred that allocating Rooms 4, 5, and 6 to post-operative patients can be avoided to monitor them efficiently. The histogram with the field strength at the static receiver point is shown in Figure 20. It is inferred that Rooms 3 and 8 are more suitable for allocating them to post-operative patients.

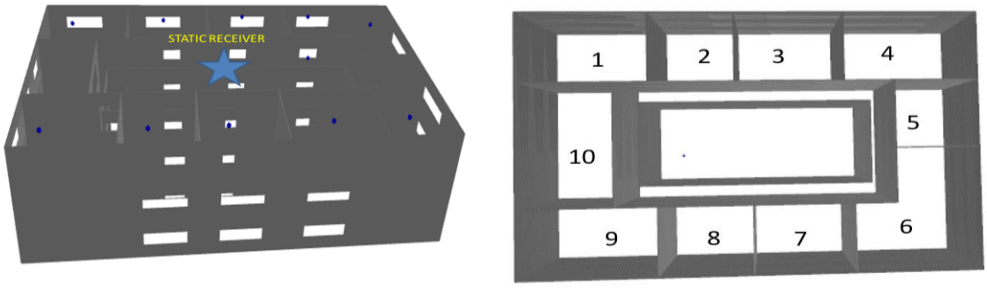


**Figure 18.** Indoor scenario with the static receiver at nursing station and rooms.

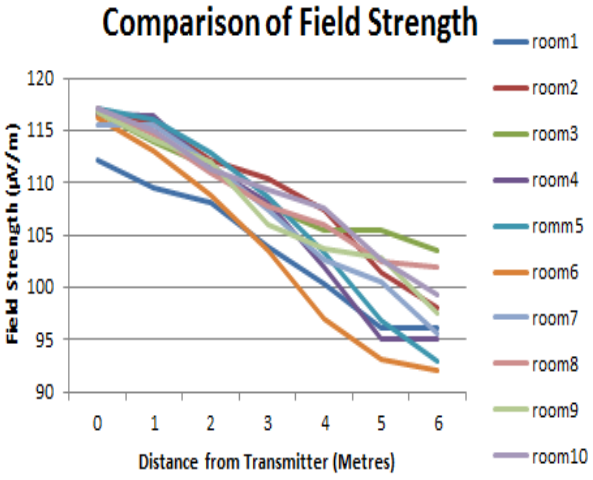


**Figure 19.** Comparison graph for field strength from the transmitter to the receiver.

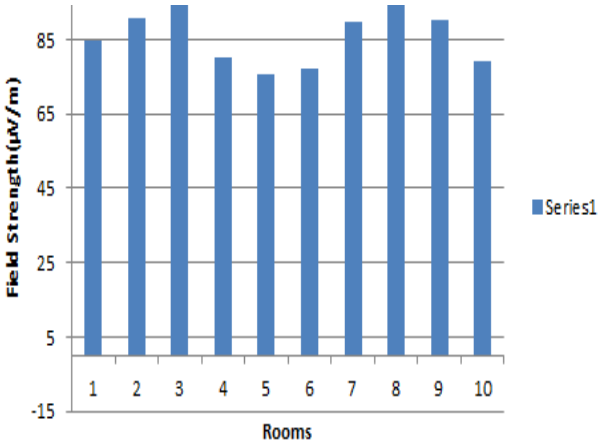


**Figure 20.** Field strength at the static receiver (centre).

### *3.4.2. Analysis of Field Strength for Mobile Receiver*

The field strength for each corner changes according to the interior building structure (doors, windows, stairs). When the receiver is moving continuously, it is checked whether it can receive the signal efficiently even at the farthest point of the hospital from the transmitter. The prediction is done at a

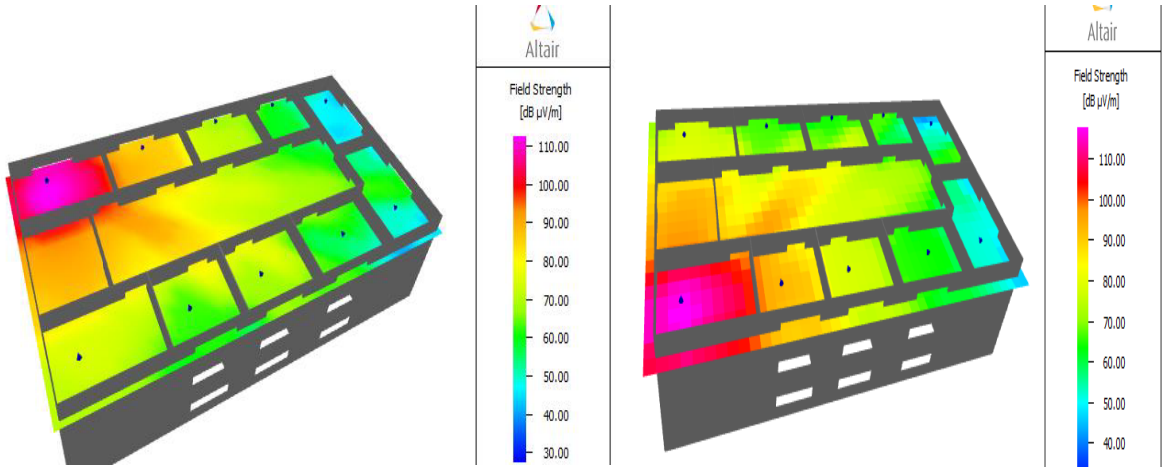


(a) (b)

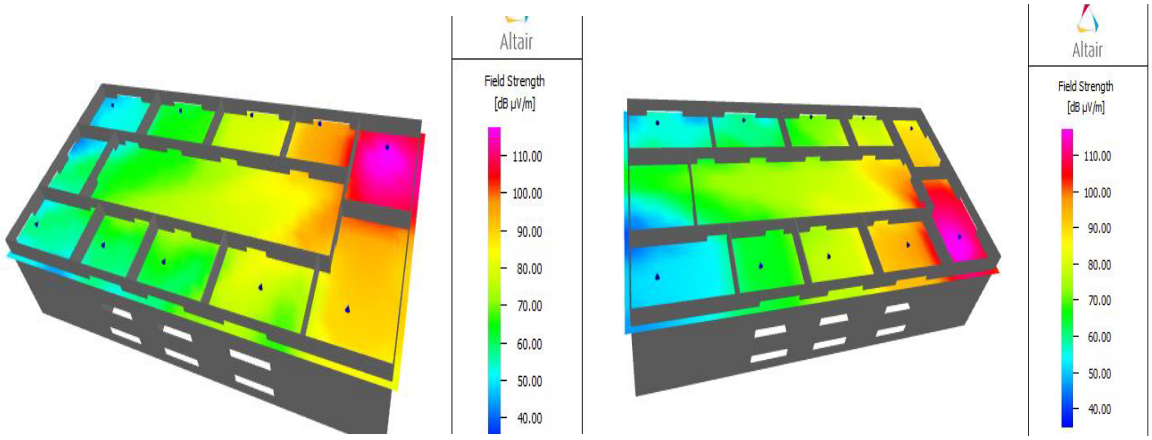


(c) (d)

**Figure 21.** Field strength for the transmitter when at various corners (third floor). (a) Top left. (b) Bottom left. (c) Top right. (d) Bottom right.

height of 7.5 m from the ground plane (Second Floor). A field strength of 60 µV/m or higher is recorded for a transmitter power of 1 mW for the left corners (top & bottom) as shown in Figures 21(a) & (b). When the analysis is done for right-hand side corners (top & bottom) a field strength lower than 60 µV/m is recorded on the farthest end (left side) of the building as shown in Figures 21(c) & (d).

A histogram for field strengths at the reference points where field strength is $< 50\,\mu V/m$ for each of the four transmitters considered for mobile receiver analysis is plotted in Figure 22. Hence, the allocation of post-operative patients to the rooms on the farthest right can be avoided.

**Table 4.** Comparison of the proposed implantable antenna with existing alternatives in the literature.

| **Citation Author (Year)** | **$f_r$ Band** | **$\varepsilon_r$** | **Radiating Patch** | **Patch Size [mm]** | **$S_{11}$ [dB]** | **Radiation efficiency [%]** | **Gain [dBi]** | **SAR limit [W/kg] $I_0$ g of tissue** |
|---|---|---|---|---|---|---|---|---|
| Izdebski et al. (2009) | 1.4 GHz | 2.2 | Planar meandered dipole | 29 × 5 ×0.13 | −18 | 11 | −26 | NA |
| NA Konstantin et al. (2013) | 402 MHz | 2.2 | meandered dipole | 18 × 18 ×0.13 | −37.5 | NA | −29.64 | Achieved by reducing the power to 3.83 mW |
| Zhang (2018) | 915 MHz | 3.5 | Diffrential-fed patch | 32 × 5.8 ×0.15 | −21 | NA | −21 | 50 mm depth |
| Suzan et al. (2013) | 433 MHz | 2.55 | Loop | 34.54 × 20.3 ×0.0001 | −27 | NA | −28 | NA |
| Kwou (2012) | 1.4 GHz | 2.2 | Meandered Strip Load | 25 × 15 ×0.13 | −22 | NA | −25.2 | NA |
| Das et al. (2017) | 402–428 MHz | 4.3 | Conformal Patch with slots | 31 × 20.5 ×0.025 | −24 | 31.5 | −34.6 | NA |
| Mary Neebha (2020) | 5.8 GHz | 3.5 | AMC based Monopole | 4.6 × 7.6 ×0.15 | −41 | 88.7 | 1.638 | 0.8350 |
| **Proposed Work** | **2.45 GHz** | **10.2** | **Meandered spiral** | **2.5 × 7 ×0.04** | **−60.57** | **51.8** | **−36.39** | **1.549** |

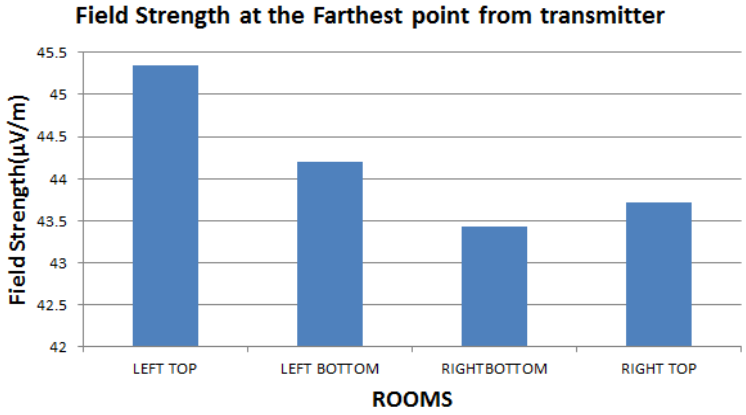


**Figure 22.** Field strength at the farthest point from the transmitter.

A comparison of the proposed implantable antenna with the existing alternatives is consolidated in Table 4.

## 4. CONCLUSION & FUTURE WORKS

The analysis can be used for efficient room allocations of post-operative patients. The room with the best field strength can be selected and reserved for patients with long-term illness. As the monitoring is wireless, interference will be a major issue. Future investigations can be carried out to mitigate the interference from nearby devices working on the same frequency for efficient monitoring of the patients. Flexibility studies can be carried out to achieve better radiation characteristics.

## CONFLICTS OF INTERESTS

The authors report no conflicts of interest.

## REFERENCES

1. Yousaf, M., I. B. Mabrouk, M. Zada, A. Akram, Y. Amin, M. Nedil, and H. Yoo, "An ultra-miniaturized antenna with ultra-wide bandwidth characteristics for medical implant systems," *IEEE Access*, Vol. 9, 40086–40097, 2021.
2. Rohei, M. S., E. Salwana, N. B. A. K. Shah, and A. S. Kakar, "Design and testing of an epidermal RFID mechanism in a smart indoor human tracking system," *IEEE Sensors Journal*, 2020.
3. Singh, H. and S. K. Mandal, "A silicon-based ferrite loaded miniaturized on-chip antenna with enhanced gain for implantable bio-telemetry applications," *Progress In Electromagnetics Research M*, Vol. 91, 69–79, 2020.
4. Karacolak, T., R. Cooper, J. Butler, S. Fisher, and E. Topsakal, "In vivo verification of implantable antennas using rats as model animals," *IEEE Antennas and Wireless Propagation Letters*, Vol. 9, 334–337, 2010.
5. Klapstova, A., J. Horakova, M. Tunak, A. Shynkarenko, J. Erben, J. Hlavata, P. Bulir, and J. Chvojka, "A PVDF electrospun antifibrotic composite for use as a glaucoma drainage implant," *Materials Science and Engineering: C*, Vol. 119, 111637, 2021.
6. Ketavath, K. N., D. Gopi, and S. S. Rani, "In-vitro test of miniaturized CPW-fed implantable conformal patch antenna at ISM band for biomedical applications," *IEEE Access*, Vol. 7, 43547–43554, 2019.

7. Golestanirad, L., M. I. Iacono, B. Keil, L. M. Angelone, G. Bonmassar, M. D. Fox, T. Herrington, et al., "Construction and modeling of a reconfigurable MRI coil for lowering SAR in patients with deep brain stimulation implants," *Neuroimage*, Vol. 147, 577–588, 2017.
8. Neebha, T. M., A. D. Andrushia, and S. Durga, "A state-of-art review on antenna designs for ingestible application," *Electromagnetic Biology and Medicine*, Vol. 39, No. 4, 387–402, 2020.
9. Rigelsford, J. M., B. F. Al-Azzawi, C. J. Davenport, and P. Novodvorsky, "A passive biodegradable implant for subcutaneous soft-tissue trauma monitoring," *IEEE Journal of Biomedical and Health Informatics*, Vol. 19, No. 3, 901–909, 2015.
10. Boutry, C. M., Y. Kaizawa, B. C. Schroeder, A. Chortos, A. Legrand, Z. Wang, J. Chang, P. Fox, and Z. Bao, "A stretchable and biodegradable strain and pressure sensor for orthopaedic application," *Nature Electronics*, Vol. 1, No. 5, 314–321, 2018.
11. Boutry, C. M., L. Beker, Y. Kaizawa, C. Vassos, H. Tran, A. C. Hinckley, R. Pfattner, et al., "Biodegradable and flexible arterial-pulse sensor for the wireless monitoring of blood flow," *Nature Biomedical Engineering*, Vol. 3, No. 1, 47–57, 2019.
12. Gardner, R. M., T. P. Clemmer, R. S. Evans, and R. G. Mark, "Patient monitoring systems," *Biomedical Informatics*, 561–591, Springer, London, 2014.
13. Baig, M. M., H. GholamHosseini, A. A. Moqeem, F. Mirza, and M. Lindén, "A systematic review of wearable patient monitoring systems — Current challenges and opportunities for clinical adoption," *Journal of Medical Systems*, Vol. 41, No. 7, 1–9, 2017.
14. Almahdi, E. M., A. A. Zaidan, B. B. Zaidan, M. A. Alsalem, O. S. Albahri, and A. S. Albahri, "Mobile patient monitoring systems from a benchmarking aspect: Challenges, open issues and recommended solutions," *Journal of Medical Systems*, Vol. 43, No. 7, 1–23, 2019.
15. Pawar, P., V. Jones, B.-J. F. Van Beijnum, and H. Hermens, "A framework for the comparison of mobile patient monitoring systems," *Journal of Biomedical Informatics*, Vol. 45, No. 3, 544–556, 2012.
16. Simha, A., S. M. Kulkarni, and S. Meenatchisundaram, "An analytical method to determine the response of a micro capacitive pressure sensor," *Sensors & Transducers*, Vol. 130, No. 7, 118, 2011.
17. International Commission on Non-Ionizing Radiation Protection, "Guidelines for limiting exposure to electromagnetic fields (100 kHz to 300 GHz)," *Health Physics*, Vol. 118, No. 5, 483–524, 2020.
18. Gabriel, S., R. W. Lau, and C. Gabriel, "The dielectric properties of biological tissues: III. Parametric models for the dielectric spectrum of tissues," *Physics in Medicine & Biology*, Vol. 41, No. 11, 2271, 1996.
19. Balanis, C. A., *Antenna Theory: Analysis and Design*, John Wiley & Sons, 2015.
20. Jasim, S. E., M. A. Jusoh, M. H. Mazwir, and S. N. S. Mahmud, "Finding the best feeding point location of patch antenna using HFSS," *ARPN Journal of Engineering and Applied Sciences*, Vol. 10, No. 23, 17444–17449, 2015.